THE ASTROPHYSICAL JOURNAL, 509:203–211, 1998 December 10

EVIDENCE FOR THE GALACTIC X-RAY BULGE. II.

SANGWOOK PARK AND JOHN P. FINLEY
Department of Physics, Purdue University, 1396 Physics Building, West Lafayette, IN 47907;
parksan@physics.purdue.edu, finley@physics.purdue.edu

AND

T. M. DAME
Harvard-Smithsonian Center for Astrophysics, 60 Garden Street, Cambridge, MA 02138; tdame@cfa.harvard.edu
Received 1998 January 23; accepted 1998 July 14

ABSTRACT

A mosaic of five *ROSAT* PSPC-pointed observations in the Galactic plane ($l \sim 25°$) reveals X-ray shadows in the 0.5–2.0 keV band cast by distant molecular clouds. The observed on-cloud and off-cloud X-ray fluxes indicate that $\sim 15\%$ and $\sim 37\%$ of the diffuse X-ray background in this direction in the 3/4 and 1.5 keV bands, respectively, originates behind the molecular gas that is located at ~ 3 kpc from the Sun. The implication of the derived background X-ray flux beyond the absorbing molecular cloud is consistent with, and lends further support to, recent observations of a Galactic X-ray bulge.

Subject headings: diffuse radiation — Galaxy: structure — ISM: clouds — ISM: structure — X-rays: ISM

1. INTRODUCTION

The origin and nature of the diffuse X-ray background (DXB) in the 0.5–2.0 keV band has been a puzzle for the last three decades. In the Galactic plane, study of the 0.5–2.0 keV band DXB is complicated by the presence of discrete Galactic emission features (e.g., supernova remnants, or SNRs) that must be accounted for in any investigation of the diffuse component. Despite the difficulties, it can be safely assumed that the 0.5–2.0 keV DXB in the plane is Galactic in origin, since extragalactic emission is completely absorbed and contributions due to unresolved stellar sources have been shown to be small (Schmitt & Snowden 1990; Wang 1992; Ottmann & Schmitt 1992). Provided that the contribution from Galactic discrete emission features can be effectively removed, the Galactic plane is then a useful laboratory for the study of the Galactic component of the DXB. One way to study the three-dimensional spatial structure of this Galactic component is to search for "shadows" cast by absorbing molecular gas at various distances and directions. The *ROSAT* XRT/PSPC, with its large field of view (2° diameter), good angular resolution (25″ on-axis), and soft X-ray bandpass (0.1–2.4 keV), is an ideal tool for this type of study. Previous studies at high Galactic latitudes utilizing the *ROSAT* PSPC (see, e.g., Snowden et al. 1991; Burrows & Mendenhall 1991; Snowden, McCammon, & Verter 1993; Wang & Yu 1995) have demonstrated the utility of the shadowing technique, which is enhanced when the absorbing cloud is at a known distance.

Recently, X-ray shadows in the DXB cast by distant molecular gas in the Galactic plane have been detected with a mosaic of *ROSAT* PSPC-pointed observations in the direction of $l \sim 10°$ (Park et al. 1997, hereafter P97). P97 detected a shadowing depth of $\sim 43\%$ in both the 3/4 and 1.5 keV bands, and the derived background intensity (beyond the absorbing molecular gas) is more than 1 order of magnitude brighter than the nominal high-latitude intensity. This striking result implies the existence of an X-ray–emitting Galactic bulge. This observation is consistent with analysis of *ROSAT* all-sky survey data in the general direction of the Galactic center (Snowden et al. 1997) where excess emission observed at high Galactic latitudes was extrapolated down to the Galactic plane. P97 determined that the de-absorbed background spectrum of the tentative Galactic X-ray bulge is consistent with a $\sim 10^{6.7}$ K thermal plasma, also in good agreement with the all-sky survey results. Here we report the detection of X-ray shadows cast by distant molecular clouds in the direction of $l \sim 25°$ in the Galactic plane.

There is probably a much more complicated mixture of X-ray emission and absorption along the line of sight toward $l \sim 25°$ than toward the $l \sim 10°$ region studied by P97. Toward $l \sim 10°$, the line of sight passes through the molecular ring and then through a long section of the Galactic center region where the density of both atomic and molecular gas is very low and the X-ray emission presumably originates (the X-ray bulge). Most of the neutral and molecular gas therefore lies in front of most of the X-ray emission, and clouds are seen clearly in silhouette. Toward $l \sim 25°$, molecular clouds are more widely distributed along the line of sight, which passes nearly tangent to the inner edge of the molecular ring and through a shorter chord of the X-ray bulge.

The data used for this study are described in § 2. The analysis and results are presented in § 3, and the implications are discussed in § 4.

2. DATA

Previous studies of the DXB using X-ray shadows cast by nearby molecular clouds have utilized the anticorrelation between the X-ray intensity and the *IRAS* 100 μm intensity (see, e.g., Burrows & Mendenhall 1991, 1994; Snowden, McCammon, & Verter 1993; Wang & Yu 1995; Kuntz, Snowden, & Verter 1997). The *IRAS* 100 μm data are a reasonable gas tracer, and the utility of these data has been demonstrated with high-latitude molecular clouds with *known* distances (e.g., Draco cloud at ~ 300 pc, Burrows & Mendenhall 1991 and Snowden et al. 1991; MBM 12 at ~ 65 pc, Snowden et al. 1993) or nearby low-latitude dense molecular clouds (e.g., the Coalsack at ~ 200 pc from the Sun, Burrows & Mendenhall 1994). However, to search for 0.5–2.0 keV band X-ray shadows cast by "distant" (greater

TABLE 1

LIST OF *ROSAT* PSPC OBSERVATIONS

Observation ID	l	b	Exposure (ks)	Date
RP 400287N00	23.34	0.18	7.80	1993 Apr 3–9
RP 500008	23.53	0.32	3.67	1991 Mar 30
RP 500012	24.66	0.61	4.26	1991 Apr 3
RP 400288N00	25.09	0.55	8.60	1993 Apr 9
WP 500204N00.....	25.52	0.22	16.84	1993 Apr 7–8

than 1 kpc) molecular clouds in the Galactic plane, the *IRAS* 100 μm data are of limited use, since there are generally many clouds overlapped along the line of sight, and with no velocity information there is no way to determine their individual distances. The *IRAS* 100 μm data can also be confused by emission from H II regions in the plane. These difficulties with the *IRAS* 100 μm data can be overcome by studying the X-ray anticorrelations with CO spectral line data, a standard tracer of interstellar molecular gas. Although CO data also have their own complications, such as the conversion between CO intensity and H column density, they clearly provide better information regarding absorbing molecular clouds in the plane. This work is thus based upon information derived from such data.

2.1. *X-Ray Data*

The soft X-ray data utilized in this study consist of five *ROSAT* (Trümper 1992) PSPC-pointed observations (see Table 1). Data from all five pointings were obtained through the High Energy Astrophysics Science Archive Research Center (HEASARC) *ROSAT* public archive. The R4, R5, R6, and R7 band data (see Snowden et al. 1994 for band definitions) are utilized in the study of the 0.5–2.0 keV band DXB in the Galactic plane. The R1L and R2 band emission, which comprise a 1/4 keV band, is assumed to have a completely different origin; i.e., the Local Hot Bubble (LHB), a region of $\sim 10^6$ K plasma surrounding the Sun with an average extent of ~ 100 pc (Cox & Reynolds 1987). This emission is thus not considered in this study.

Since noncosmic contamination must be carefully handled when studying the DXB, all identified noncosmic contributions to the counting rate must be excluded by time selection or modeled and subtracted from the data. We modeled and subtracted the particle background, scattered solar X-ray background, and long-term enhancements from the data. A detailed description of the noncosmic background subtraction methods can be found in the literature (Snowden et al. 1994). We also eliminated contamination due to short-term enhancements including auroral X-rays, solar flares, and enhanced charged-particle rates encountered near the South Atlantic Anomaly and particle belts by excluding all observation time intervals that display anomalous peaks in their light curves. For these five pointings, the mean contribution of the modeled noncosmic contamination to the counts is $\sim 13\%$ in the 0.5–2.0 keV band. We removed the detected point sources and extended discrete emission features (e.g., SNRs) from the data prior to the DXB analysis. Unresolved point sources are expected to provide only a minor contribution to the surface brightness.

After all identified noncosmic contamination, detected point sources, and discrete extended emission features are removed, the individual PSPC pointings are merged into large-area mosaics in two bands: the 3/4 keV band (R4 plus R5) and the 1.5 keV band (R6 plus R7). The determination of the relative offsets in the zero level between the individual observations is performed by comparing the average count rates in the overlapping regions between all pairs of observations. The contribution from this correction is typically small ($\sim 2\%$ and $\sim 3\%$ of the total counts in the 3/4 and 1.5 keV bands, respectively) for the entire field of view. The software for this task (Snowden 1994) was provided by the US *ROSAT* Science Data Center (USRSDC) at NASA/GSFC.

The final *ROSAT* PSPC mosaics of the $l \sim 25°$ direction of the Galactic plane are displayed in Figures 1*a* (the 3/4 keV band) and 1*b* (the 1.5 keV band). For the purpose of display, the data were smoothed to 7.5 resolution in order to match the resolution of the CO data used. The circles in Figure 1*a* indicate the 10 regions where detected bright point sources and discrete extended emission features have been removed. Combined as a mosaic, the average exposure for this field is ~ 9 ks, which yields $\sim 16\%$ (1.5 keV band) and $\sim 20\%$ (3/4 keV band) statistical errors for individual 5′ pixels.

2.2. CO *Data*

The CO data used in the present study were obtained with the CfA 1.2 m telescope as part of a large ongoing survey of the first Galactic quadrant (Dame & Thaddeus 1994). At 115 GHz, the frequency of the $J = 1$–0 rotational transition, the telescope has a beamwidth of 8.4 (FWHM) and its 256 channel spectrometer provides a velocity resolution of 0.65 km s^{-1} and total bandwidth of 166 km s^{-1}. Observations were spaced roughly every beamwidth (7.5) on a Galactic grid, and the rms sensitivity of 0.14 K ($T_{\rm mb}$) was more than adequate for the present purpose.

3. ANALYSIS AND RESULTS

Figure 2 compares the 1.5 keV band X-ray image with contours of CO intensity integrated over three different ranges of velocity. For the clarity of the presentation of the CO intensity variation, gray-scale CO images for the same three velocity intervals are displayed in Figure 3. The overall anticorrelation between the X-ray and the CO intensities, as presented in Figure 2, reveals several X-ray shadows. These X-ray shadows are indicated by solid-lined rectangles in Figure 1*b* and labeled as A, B, C, and D.

Shadow A at $l, b \sim 23.5, 0°$ appears to arise mainly from a molecular cloud at a velocity of ~ 54 km s^{-1} (Fig. 2*b*) for which the near kinematic distance is ~ 3.8 kpc. Despite the clear shadowing feature in this region, a detailed analysis of shadow A is unwarranted because of the difficulty in extracting a meaningful off-cloud surface brightness (see below for more discussion).

It is notable that a much more intense CO feature at l, $b \sim 23.4$, -0.35 in the $V = 55$–130 km s^{-1} map (Fig. 2*c*) does not produce any noticeable X-ray shadow. This intense CO feature is believed to be a large star-forming cloud at the far kinematic distance ($d \sim 13$ kpc; Dame et al. 1986). Assuming that the bulk of the detected diffuse X-ray emission is originating from within or foreground to the Galactic X-ray bulge, no detected shadow by this CO enhancement is reasonable since this cloud should be located behind the 0.5–2.0 keV band X-ray–emitting region.

Shadow B at $l, b \sim 24.6, 0°$ seems to be associated with the molecular clouds in the velocity interval $V = 30$–55 km s^{-1} (Fig. 2*b*), which corresponds to a near kinematic dis-

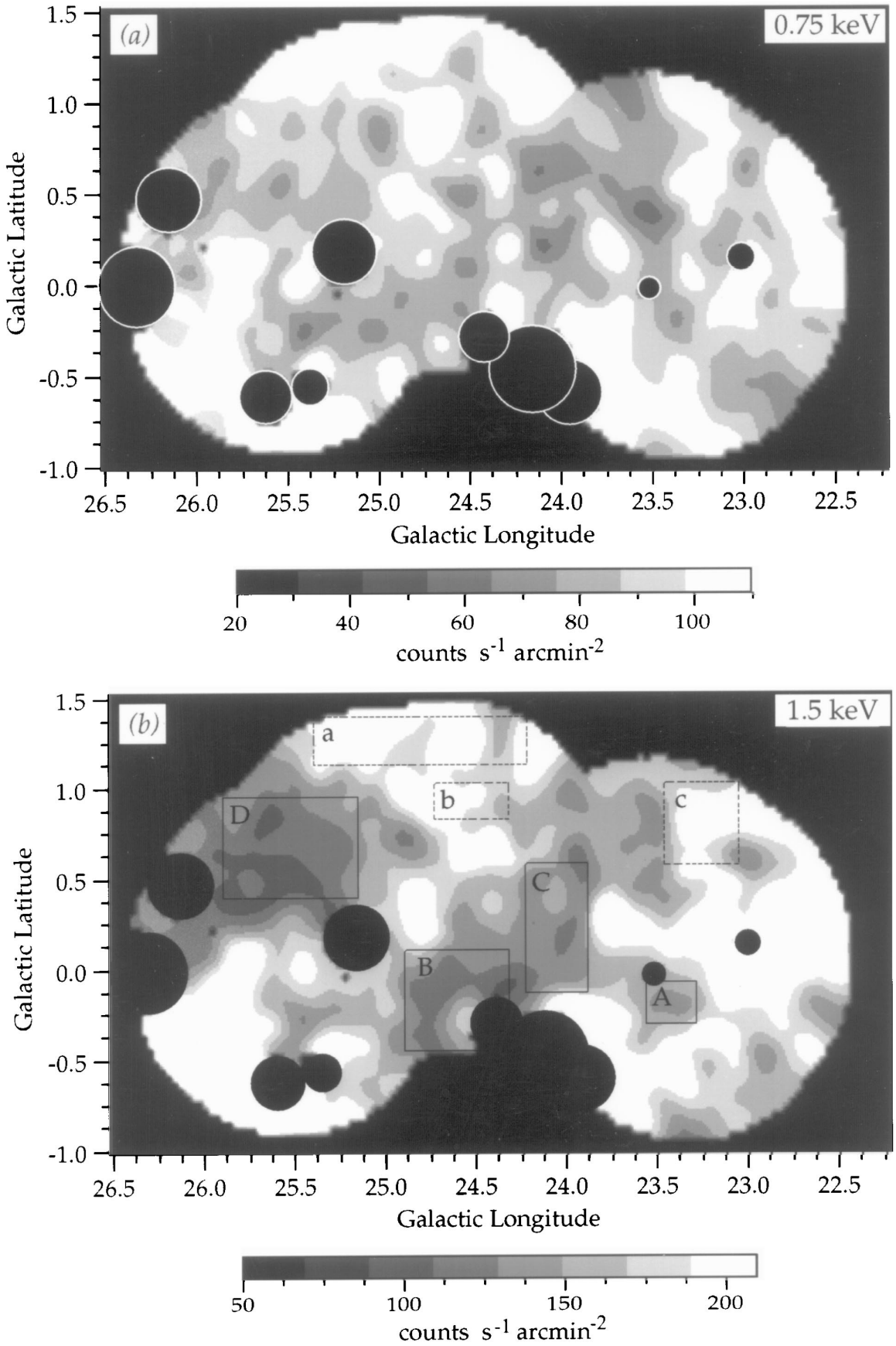

FIG. 1.—X-ray images of the Galactic plane near $l \sim 25°$. These cover an area of ~ 10 deg^2 between $l = 22.°5$ and $l = 26.°5$ at $b \leq 1.°5$. (*a*) and (*b*) display the 3/4 and 1.5 keV X-ray images, respectively, from the mosaic of the five *ROSAT* PSPC-pointed observations in Table 1. The circles indicate the regions where the detected bright point sources and discrete extended emission features are removed. For the purpose of display, the data have been smoothed using a Gaussian with $\sigma = 7.'5$ (FWHM) to match the resolution of the CO data. (*b*) X-ray shadows A, B, C, and D are indicated by solid-lined rectangles. The off-cloud regions a, b, and c are indicated by dotted rectangles.

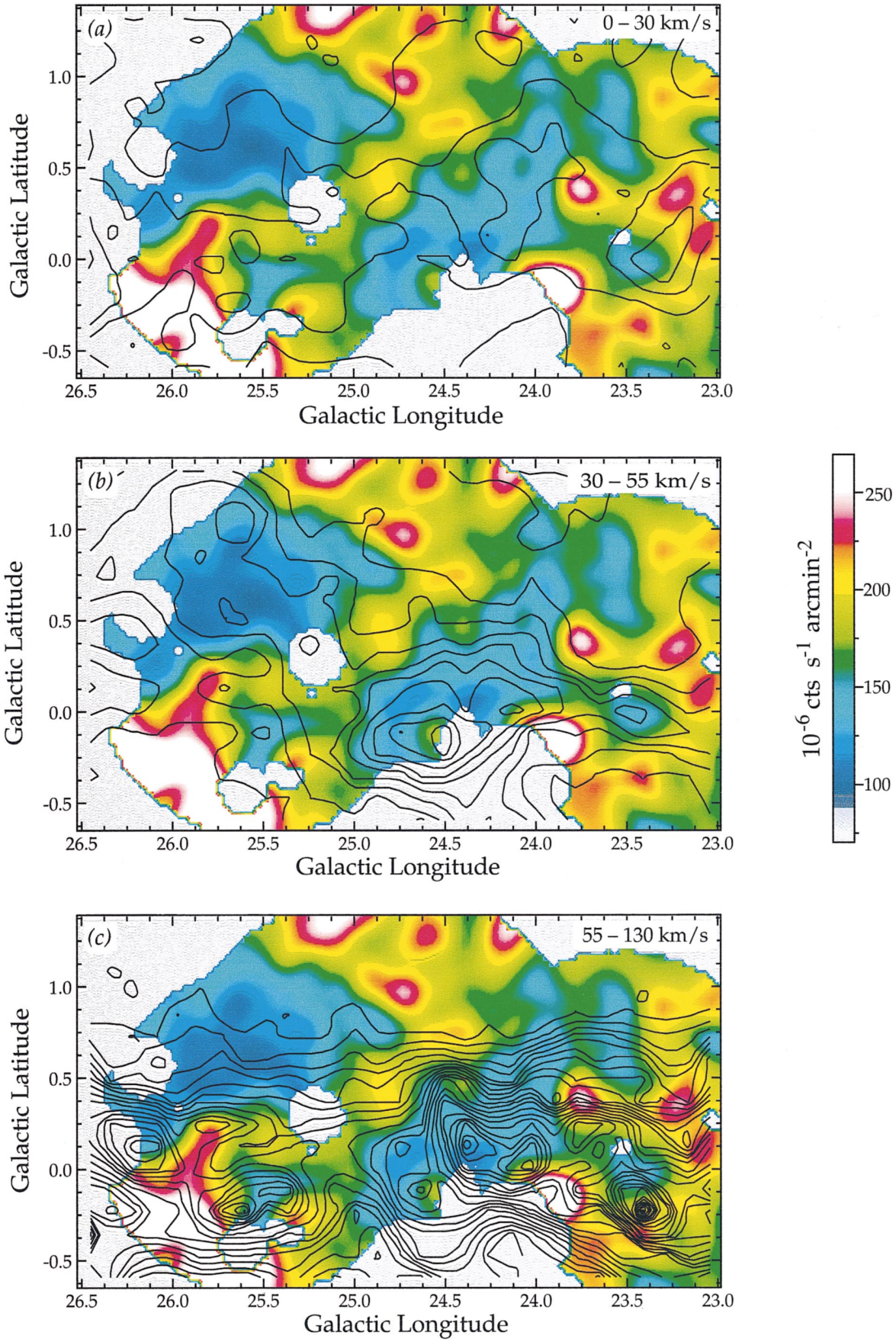

FIG. 2.—^{12}CO ($J = 1$–0) intensity in three different velocity intervals overlaid on the image of the 1.5 keV band X-rays. The CO contour interval is 7 K km s^{-1} starting at 7 K km s^{-1}. The contour at 7 K km s^{-1} corresponds to $\sim$0.6 optical depths in the 3/4 keV band, and $\sim$0.4 optical depths in the 1.5 keV band. The CO velocity integration range is given above each plot. A small portion of the X-ray map at $l < 23°$ is excluded because comparable quality CO data was not available there.

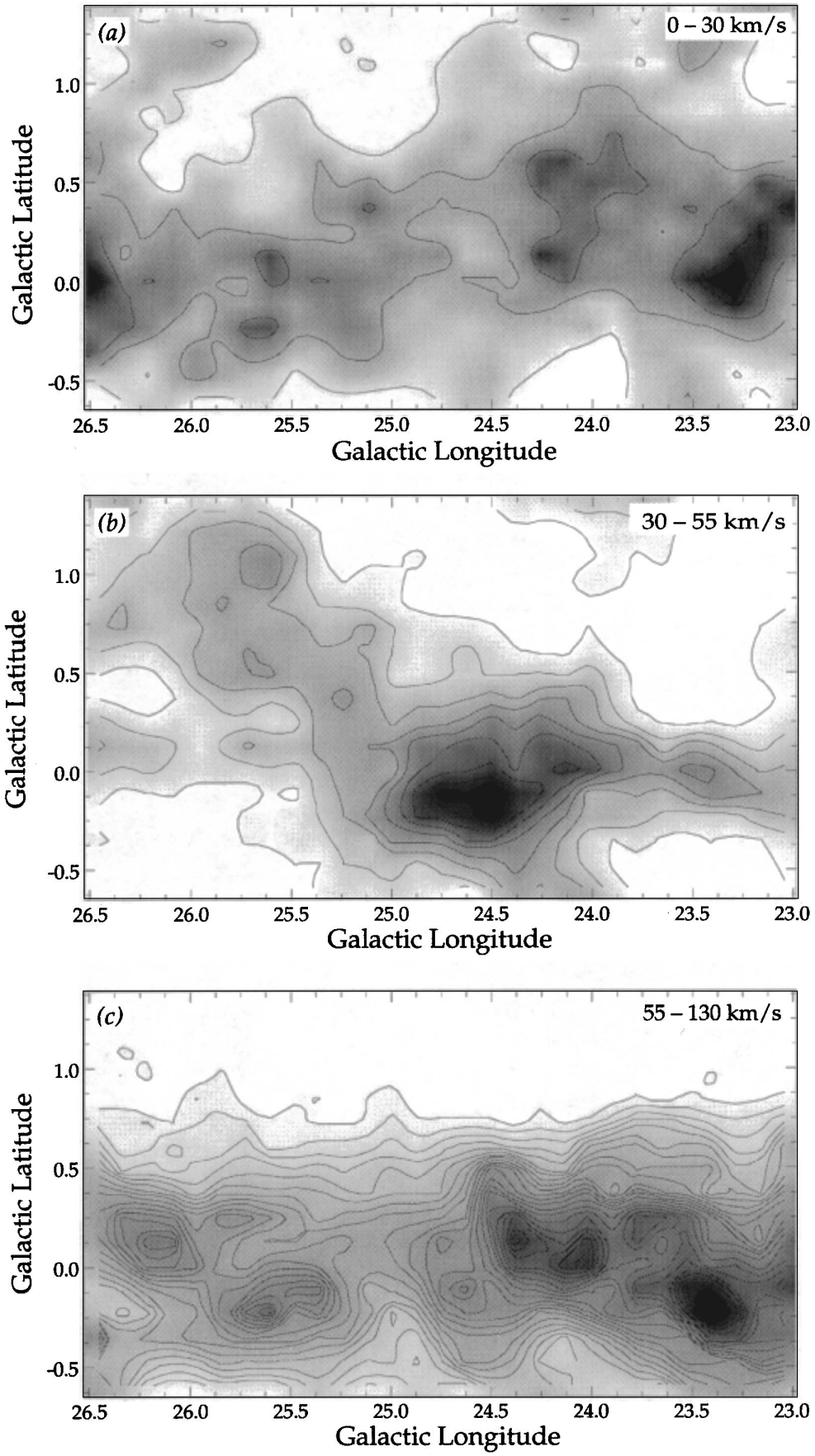

FIG. 3.—Gray-scale CO image with the overlaid contours. The three velocity intervals and the contour levels are the same as in Fig. 2.

tance of ~3 kpc. The molecular clouds in the velocity interval 55–130 km s^{-1}, however, seem to contribute substantially to this shadow as well (Fig. 2*c*). This complexity may arise from the existence of numerous molecular clouds along this line of sight due to the Galactic structure in this direction. As a matter of fact, the velocity-integrated CO intensity in the region of shadow B ($l, b \sim 24°–25°, 0°$) is the strongest in the entire Galaxy outside of the Galactic center (Dame et al. 1987).

The origin of shadow C is unclear. The CO intensity in this region is relatively strong in the velocity range of 30–130 km s^{-1} (Figs. 2*b* and 2*c*), but Figure 2*a* suggests that lower velocity gas may also contribute to the shadow, which would be reasonable since at least some of the gas is likely to be nearby.

Shadow D at $l, b \sim 25.^{\circ}5, 0.^{\circ}7$ is the most remarkable. There is a clear anticorrelation between this feature and a well-defined molecular cloud at $V = 46$ km s^{-1} (Fig. 2*b*). With a near kinematic distance of 3.3 kpc (Fig. 4), the molecular cloud extends fairly high above the Galactic plane ($z \sim 70$ pc at 3.3 kpc, $z \sim 250$ pc at the far kinematic distance, 12.2 kpc), where there is much less foreground or background molecular gas but still a bright X-ray background. Shadow D is thus the most appropriate for a detailed quantitative analysis of the X-ray absorption. Applying a CO-H_2 conversion factor $N(H_2)/W_{CO} = 1.9 \times 10^{20}$ cm^{-2} (K km $s^{-1})^{-1}$ (Strong & Mattox 1996), the H_2 column density corresponding to the mean W_{CO} within the shadow D region is $\sim 5.4 \times 10^{21}$ cm^{-2} for the CO cloud at ~3 kpc. This column density implies that the absorbing molecular cloud at 3 kpc in this region is relatively optically thick for the 0.5–2.0 keV band X-rays since one optical depth is $\sim 2.7 \times 10^{21}$ cm^{-2} and $\sim 4.0 \times 10^{21}$ cm^{-2} in the 3/4 and 1.5 keV bands, respectively, assuming the theoretical absorption cross section of Morrison & McCammon (1983) and a $10^{6.7}$ K thermal plasma with a foreground $N_H \sim 9 \times 10^{21}$ cm^{-2} (to correct for the hardening of the X-ray bulge spectrum by the foreground ISM).

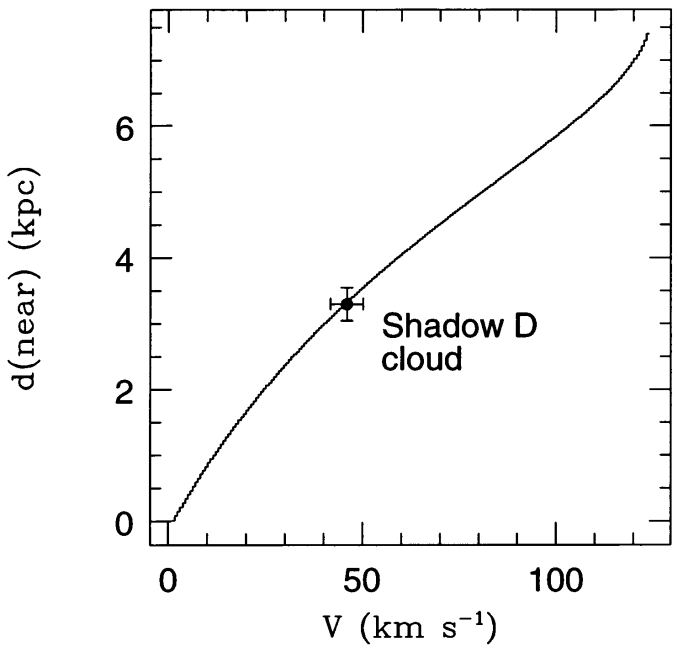

FIG. 4.—Near-kinematic distance vs. radial velocity in the direction of l, $b = 24.^{\circ}5, 0°$, based on the rotation curve of Burton (1992).

We thus directly extract the on-cloud and off-cloud X-ray intensities in order to estimate the foreground and the background (behind the molecular cloud) fractions of the observed X-ray intensity rather than fitting the standard two-component absorption model (see, e.g., Snowden et al. 1993).

The average on-cloud 1.5 keV band X-ray intensity for shadow D is $(121 \pm 2) \times 10^{-6}$ counts s^{-1} $arcmin^{-2}$. Due to the presence of many molecular clouds in the plane ($|b| \lesssim 0.^{\circ}5$) at all velocities along the line of sight, extracting off-cloud intensities within $|b| \sim 0.^{\circ}5$ of the Galactic plane is not feasible near $l \sim 25°$. The off-cloud 1.5 keV band X-ray intensity is thus estimated in the areas of the three dotted rectangular regions labeled a–c in Figure 1*b*, where $I_{CO} < 7$ K km s^{-1} (i.e., H_2 column density less than 1.3×10^{21} cm^{-2}) in Figure 2*b*. The off-cloud intensities are (203 ± 6), (198 ± 8), and $(177 \pm 6) \times 10^{-6}$ counts s^{-1} $arcmin^{-2}$ for regions a, b, and c, respectively. Combining data from the off-cloud X-ray regions yields an off-cloud intensity of $(192 \pm 4) \times 10^{-6}$ counts s^{-1} $arcmin^{-2}$.

In the 3/4 keV band, the on-cloud and the off-cloud X-ray intensities are extracted from the same regions as in the 1.5 keV band. The average on-cloud 3/4 keV band X-ray intensity is $(87 \pm 2) \times 10^{-6}$ counts s^{-1} $arcmin^{-2}$. The off-cloud intensities are (113 ± 4), (96 ± 6), and $(97 \pm 4) \times 10^{-6}$ counts s^{-1} $arcmin^{-2}$ for regions a, b, and c, respectively. Combining the data from the off-cloud regions yields an off-cloud X-ray intensity of $(102 \pm 3) \times 10^{-6}$ counts s^{-1} $arcmin^{-2}$. The observed on-cloud and off-cloud X-ray intensities in the 3/4 and 1.5 keV bands are summarized in Table 2. The errors for the on-cloud and off-cloud X-ray intensities in both 3/4 and 1.5 keV bands are formal statistical uncertainties, and any systematic errors such as uncertainty due to the selection of the extraction regions will increase the uncertainties presented here.

The average on-cloud to off-cloud X-ray intensity ratio in the 1.5 keV band is 0.63 ± 0.02, which implies a ~37% contribution to the observed diffuse X-ray background from beyond the molecular cloud. Using H I and CO spectra toward the off-cloud regions, the foreground column density is estimated to be $\sim 7.4 \times 10^{21}$ H I cm^{-2}, $\sim 11.1 \times 10^{21}$ H I cm^{-2}, and $\sim 12.7 \times 10^{21}$ H I cm^{-2} for regions a, b, and c, respectively. The H I spectrum from the 21 cm survey of Hartmann & Burton (1997) (angular resolution of $0.^{\circ}5$) was utilized for the estimation. To derive total gas column densities along the line of sight, 21 cm and CO emissions were partitioned between the near and far kinematic distances based on assumed constant scale heights of 220 (Lockman 1984) and 120 pc (Bronfman et al. 1988), respectively. The average foreground column density for the off-cloud regions is 10.4×10^{21} H I cm^{-2} and corre-

TABLE 2

SHADOW D X-RAY FLUXES

Band	On-Cloud[a]	Off-Cloud[a]	Ratio	Off-Cloud N_H[b]
3/4 keV.....	87 ± 2	102 ± 3	0.85 ± 0.03	$10.4^{+2.3}_{-3.0}$
1.5 keV.....	121 ± 2	192 ± 4	0.63 ± 0.02	$10.4^{+2.3}_{-3.0}$

[a] On-cloud and off-cloud fluxes in units of 10^{-6} counts s^{-1} $arcmin^{-2}$. The on-cloud flux is averaged over rectangle D in Fig. 1*b*, and the off-cloud flux is averaged over rectangles a, b, and c in Fig. 1*b*. The errors are the formal statistical uncertainty.

[b] The average foreground column density of the off-cloud regions a, b, and c in units of 10^{21} cm^{-2}.

sponds to a foreground absorption optical depth in the 1.5 keV band X-rays of $\tau \sim 2.6$. After deabsorption, this implies a background intensity of $(956 \pm 25) \times 10^{-6}$ counts s^{-1} $arcmin^{-2}$, even without any correction for possible absorption by material beyond the cloud but foreground to the X-ray–emitting region. This value is, on average, about a factor of 7 higher than the nominal high-latitude intensity ($\sim 130 \times 10^{-6}$ counts s^{-1} $arcmin^{-2}$).

The average on-cloud to off-cloud X-ray intensity ratio in the 3/4 keV band is 0.85 ± 0.03, which implies that $\sim 15\%$ of the observed X-ray emission is from behind the molecular cloud. The foreground absorption optical depth in the 3/4 keV band X-ray is $\tau \sim 3.9$, and the estimated background intensity is $(741 \pm 28) \times 10^{-6}$ counts s^{-1} $arcmin^{-2}$. The derived average background intensity in this energy band is also higher (by a factor of 6) than the nominal high-latitude intensity.

4. DISCUSSION

The derived average background X-ray intensities in both the 1.5 and 3/4 keV bands are larger than the nominal high-latitude intensity by a factor of 6–7, indicating an extensive region of X-ray–emitting Galactic gas beyond the absorbing molecular cloud located at ~ 3 kpc. The implied DXB emission is consistent with the existence of an emission region near the Galactic center as posited by P97 in connection with X-ray shadows observed in the direction of $l \sim 10°$ and a Galactic X-ray bulge suggested by Snowden et al. (1997) based on *ROSAT* all-sky survey data. The derived background X-ray intensity (assuming no further absorption behind the molecular cloud) in the $l \sim 25°$ direction, however, appears to be lower than that of P97 ($\sim 65\%$ of P97 in the 1.5 keV band and $\sim 30\%$ of P97 in the 3/4 keV band, on average). The lower values of the derived background intensity are not surprising and are likely related to the spatial structure of the Galactic X-ray bulge in the plane, in that the $l \sim 25°$ direction is closer to the "edge" of the Galactic X-ray bulge and therefore the path length through the emission region will be shorter. Considering the Galactic molecular gas distribution (i.e., the molecular ring; see below for more discussion), the path length difference through the X-ray bulge between the directions of P97 ($l \sim 10°$) and the present paper ($l \sim 25°$) is expected to produce less than a 50% background X-ray intensity in the $l \sim 25°$ direction (Fig. 5).

The lower intensity of the DXB behind the absorbing molecular cloud and the relatively shallow shadowing depths compared with P97 may also be because of an increase in the interstellar absorption beyond 3 kpc. This speculation is reasonable when the morphology of the prospective Galactic X-ray bulge in the *ROSAT* all-sky survey maps (the highly enhanced X-ray–emission feature around

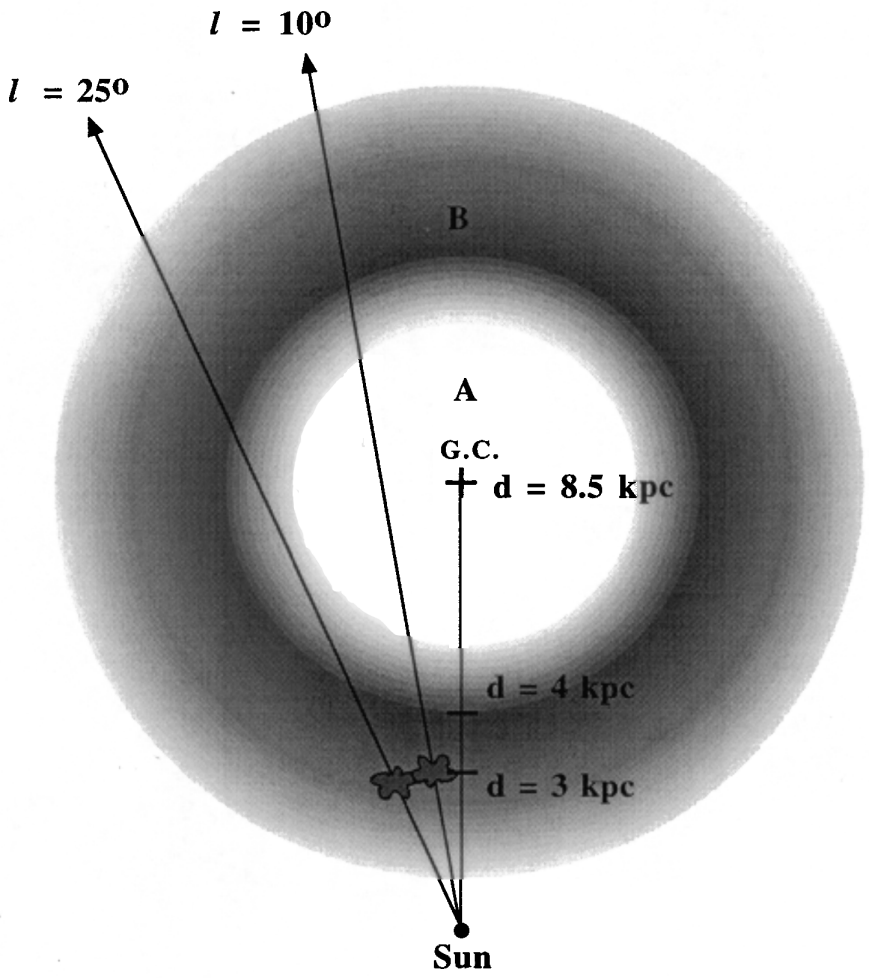

FIG. 5.—Schematic diagram for the simplistic geometry of the Galactic X-ray bulge and the molecular ring in the plane. Region A represents the void that is filled with the X-ray–emitting gas (Galactic X-ray bulge). Region B is the molecular ring. The $l \sim 25°$ direction skims the inner edge of the molecular ring while the $l \sim 10°$ direction passes through the X-ray bulge.

the Galactic center region; see Snowden et al. 1997) and the Galactic structure of molecular gas (see § 1) are considered. If the weaker shadows and the lower DXB intensity are due to additional interstellar absorption beyond 3 kpc, the additional absorbing background ISM can be estimated using a simple absorption model. Assuming a negligible interstellar absorption of the X-ray bulge emission beyond the shadow-casting molecular clouds in the $l \sim 10°$ direction, the difference in the derived background X-ray intensities between $l \sim 10°$ and $l \sim 25°$ (assuming the average shadowing depths) requires an additional Galactic interstellar absorption of $N_{\rm H} \sim 3.2 \times 10^{21}$ cm^{-2} beyond 3 kpc in the $l \sim 25°$ direction. Assuming a foreground column density of 9.6×10^{21} cm^{-2} in the direction of shadow D as estimated from the H I and CO spectra, the derived total $N_{\rm H}$ (foreground plus background of the shadow-casting molecular cloud) in the $l \sim 25°$ direction is $\sim 13 \times 10^{21}$ cm^{-2}. For comparison, an analysis of the CO and H I spectra indicates that there should be $N_{\rm H}$ of 6.7×10^{21} cm^{-2} between 4 and 8 kpc toward the center of shadow D (l, $b = 25.^{\circ}5$, $0.^{\circ}75$). The corresponding total $N_{\rm H}$ is then $\sim 16 \times 10^{21}$ cm^{-2}. From the CO and H I surveys (Hartmann & Burton 1997), the total $N_{\rm H}$ is estimated to be $18–45 \times 10^{21}$ cm^{-2} in this direction, which is consistent with the derived total $N_{\rm H}$.

As determined by the Galactic CO gas distribution, the inner edge of the molecular ring is located at $l \sim 25°$ in the plane. The Galactic X-ray bulge then appears confined by the molecular ring, at least in the plane, since it extends to only $l \sim 25°$ in the first quadrant of the plane (Snowden et al. 1995). By comparison, in the $l \sim 10°$ direction, the implied background fraction of the DXB likely originates within the void that is interior to the molecular ring. The velocity intervals of the absorbing gas identified as shadows in the DXB (i.e., 15–30 km s^{-1} at $l \sim 10°$, P97; 30–55 km s^{-1} at $l \sim 25°$, the present paper) in fact track the molecular ring structure (Dame et al. 1987). The coincidence of the distance scales for the absorbing molecular gas ($\sim$3 kpc from the Sun) in the directions of both P97 and the present paper with the location of the molecular ring ($\sim$3–4 kpc from the Sun at its closest approach) indicates that all of these X-ray shadows are cast by molecular clouds associated with the Galactic molecular ring.

The 1.5-3/4 keV band hardness ratio for the average derived background emission is 1.29 ± 0.06 (with no further absorption). This hardness ratio is higher than that of P97 (0.59 ± 0.16). The harder spectrum is consistent with the existence of additional interstellar absorption beyond 3 kpc. Assuming the additional absorption is $N_{\rm H} \sim 3.2–6.7 \times 10^{21}$ cm^{-2}, the average 1.5-3/4 keV hardness ratio of the "deabsorbed" spectrum is then $\sim$0.58–0.88, which is closer to the value of P97. These hardness ratios suggest a plasma temperature of the derived background X-ray emission of $T \gtrsim 10^{6.7}$ K.

5. SUMMARY AND CONCLUSIONS

We have presented an analysis of X-ray shadows in the 0.5–2.0 keV band diffuse X-ray background in the Galactic plane cast by dense molecular clouds in the direction of $l \sim 25°$, and we have discussed the implications of the results. The average on-cloud and off-cloud X-ray intensities imply that $\sim$37% of the observed 1.5 keV band and $\sim$15% of the 3/4 keV band diffuse X-rays originate from beyond 2.6–3.9 optical depths. The average derived background emission beyond $\sim$3 kpc is a factor of 5–7 higher than the nominal high-latitude intensity, even with no additional absorption, and confirms the existence of the Galactic X-ray bulge (P97; Snowden et al. 1997). The intensity of the derived background emission, however, appears to be lower than that of P97. This lower intensity is likely a result of the structure of the Galaxy where the $l \sim 25°$ direction of the plane (the present paper) is near the *edge* of the Galactic X-ray bulge, while the $l \sim 10°$ direction (P97) is more toward the *center* of the X-ray bulge. The morphology of the highly enhanced diffuse X-ray emission around the Galactic center region of the *ROSAT* all-sky survey maps (Snowden et al. 1995) support this suggested angular extension of the Galactic X-ray bulge. The distance scales to the absorbing clouds producing the X-ray shadows and the angular extension of the Galactic X-ray bulge may imply that the three-dimensional structure of the Galactic X-ray bulge is associated with, and likely confined by, the Galactic molecular ring, at least in the Galactic plane.

The Galactic X-ray bulge most likely contributes a substantial fraction of the observed soft X-ray background in the Galactic plane. Detailed spatial and spectral studies are needed to understand its nature and origin. The question of the nature of the soft X-ray background making up the foreground flux to the absorbing clouds (which may also be responsible for the nonzero flux in the Galactic anticenter direction) still remains unanswered. Follow-up observations of the detected X-ray shadows presented in this paper and P97 (on-cloud and off-cloud regions), and a search for more X-ray shadows cast by molecular clouds at various distances and directions, will help unveil the multicomponent structure of the soft X-ray background in the Galactic plane.

The authors thank S. Snowden for helpful comments and suggestions for the clarity of the presentations in this paper. This research has made use of data obtained through the High Energy Astrophysics Science Archive Research Center Online Service, provided by the NASA–Goddard Space Flight Center, and was supported in part by NASA grants NAG 5-2492 and NAG 5-3426, and by the Purdue Research Foundation.

REFERENCES

Bronfman, L., Cohen, R. S., Alvarez, H., May, J., & Thaddeus, P. 1988, ApJ, 324, 248
Burrows, D. N., & Mendenhall, J. A. 1991, Nature, 351, 629
———. 1994, in AIP Conf. Proc. 313, Soft X-Ray Cosmos, ed. E. Schlegel & R. Petre (New York: AIP), 16
Burton, W. B. 1992, Saas-Fee Lecture Notes (Berlin: Springer), 53
Cox, D. P., & Reynolds, R. J. 1987, ARA&A, 25, 303
Dame, T. M., Elmegreen, B. G., Cohen, R. S., & Thaddeus, P. 1986, ApJ, 305, 892
Dame, T. M., et al. 1987, ApJ, 322, 706
Dame, T. M., & Thaddeus, P. 1994, ApJ, 436, L173
Hartmann, D., & Burton, W. B. 1997, Atlas of Galactic Neutral Hydrogen (Cambridge: Cambridge Univ. Press)
Kuntz, K. D., Snowden, S. L., & Verter, F. 1997, ApJ, 484, 245
Lockman, F. 1984, ApJ, 283, 429
Morrison, R., & McCammon, D. 1983, ApJ, 270, 119
Ottmann, R., & Schmitt, J. H. M. M. 1992, A&A, 256, 421
Park, S., Finley, J. P., Snowden, S. L., & Dame, T. M. 1997, ApJ, 476, L77 (P97)
Schmitt, J. H. M. M., & Snowden, S. L. 1990, ApJ, 361, 207

Snowden, S. L. 1994, Cookbook for Analysis Procedures for *ROSAT* XRT/PSPC Observations of Extended Sources and the Diffuse Background, HEASARC/USRSDC, GSFC
Snowden, S. L., et al. 1995, ApJ, 454, 643
———. 1997, ApJ, 485, 125
Snowden, S. L., McCammon, D., Burrows, D. N., & Mendenhall, J. A. 1994, ApJ, 424, 714
Snowden, S. L., McCammon, D., & Verter, F. 1993, ApJ, 409, L21
Snowden, S. L., Mebold, U., Hirth, W., Herbstmeier, U., & Schmitt, J. H. M. M. 1991, Science, 252, 1529
Strong, A. W., & Mattox, J. R. 1996, A&A, 308, L21
Trümper, J. 1992, QJRAS, 33, 165
Wang, Q. D. 1992, ApJ, 392, 509
Wang, Q. D., & Yu, K. C. 1995, AJ, 109, 698